




Optomechanical resonator-enhanced atom interferometry

Logan L. Richardson^{1,2}, Ashwin Rajagopalan¹, Henning Albers¹, Christian Meiners¹, Dipankar Nath¹, Christian Schubert^{1,3}, Dorothee Tell¹, Étienne Wodey ¹, Sven Abend¹, Matthias Gersemann¹, Wolfgang Ertmer^{1,3}, Ernst M. Rasel¹, Dennis Schlippert ¹✉, Moritz Mehmet⁴, Lee Kumanchik^{5,6}, Luis Colmenero^{5,6}, Ruven Spannagel^{5,6}, Claus Braxmaier^{5,6} & Felipe Guzmán ^{2,5,6,7}✉

Matter-wave interferometry and spectroscopy of optomechanical resonators offer complementary advantages. Interferometry with cold atoms is employed for accurate and long-term stable measurements, yet it is challenged by its dynamic range and cyclic acquisition. Spectroscopy of optomechanical resonators features continuous signals with large dynamic range, however it is generally subject to drifts. In this work, we combine the advantages of both devices. Measuring the motion of a mirror and matter waves interferometrically with respect to a joint reference allows us to operate an atomic gravimeter in a seismically noisy environment otherwise inhibiting readout of its phase. Our method is applicable to a variety of quantum sensors and shows large potential for improvements of both elements by quantum engineering.

¹ Leibniz Universität Hannover, Institut für Quantenoptik, Welfengarten 1, 30167 Hannover, Germany. ² College of Optical Sciences, University of Arizona, Tucson, AZ 85721, USA. ³ German Aerospace Center (DLR) – Institute for Satellite Geodesy and Inertial Sensing, Hannover, Germany. ⁴ Leibniz Universität Hannover, Institut für Gravitationsphysik / Max-Planck-Institut für Gravitationsphysik (Albert-Einstein-Institut), Callinstraße 38, 30167 Hannover, Germany. ⁵ German Aerospace Center (DLR) – Institute of Space Systems, Bremen, Germany. ⁶ University of Bremen – Center of Applied Space Technology and Microgravity (ZARM), Robert-Hooke-Straße 7, 28359 Bremen, Germany. ⁷ Department of Aerospace Engineering & Physics, Texas A&M University, College Station, TX 77843, USA. ✉email: schlippert@iqo.uni-hannover.de; guzman@tamu.edu

The ability to coherently manipulate massive particles by means of interaction with light has given rise to a variety of realisations of matter-wave interferometers. Today, these are widely employed in metrology and tests of fundamental physics^{1–16}. Especially the class of interferometers based on light pulses, first pioneered by Kasevich and Chu¹⁷, finds a broad range of applications in inertial sensing^{18–29}. In these measurements, the phase reference is usually realised by a mirror retroreflecting the light pulses towards the matter waves. Inertial effects acting on the matter waves and on the phase reference are indistinguishable. As a result, seismic noise contributes significantly to the instability of atomic inertial sensors, and is even the dominant noise source in state-of-the-art matter-wave gravimeters^{19,21}. As a countermeasure, besides vibration isolation systems, commercial sensors have been exploited to track the motion of atom interferometers' inertial references, thus extending the measurement dynamic range, suppressing vibration noise^{30–35}, and allowing for comparisons with other atom interferometers^{21,36,37}.

In recent years, developments in the quantum engineering of optomechanical resonators have yielded devices with exciting applications in fields such as quantum information, fundamental physics and, likewise, in inertial sensing^{38,39}. To this end, optically reading out length variations of an optical cavity allows determination of acting accelerations with high bandwidth and resolution. In addition, interfaces between cold atoms and micromechanical cantilevers⁴⁰ or nanomembranes⁴¹ have been demonstrated, showing the potential of these hybrid systems for fundamental physics.

Here, we combine a high-bandwidth optomechanical resonator with a long-term stable light-pulse atom interferometer, and measure the accelerations of the resonator's test mass and a freely falling cloud of atoms relative to the atom interferometer's inertial reference. Our atom interferometer measures gravity under strong seismic perturbations without loss of phase information. In contrast to previous approaches, our method merges two systems both benefiting from the large toolbox of methods usually exploited in optical spectroscopy and photonics into a highly customisable device for atom interferometry in rough environments.

Results and discussion

We operate a Kasevich–Chu interferometer¹⁷ combined with an optomechanical resonator attached to the mirror providing the phase reference for the interferometer as a gravimeter (Fig. 1a, b and details in the “Methods” section). Ambient vibrational noise couples to the retroreflector at a weighted acceleration level of 3 mm s^{-2} per cycle. This leads to phase excursions exceeding a single fringe during one interferometric measurement with the readout appearing to be random due to the underlying 2π phase ambiguity (Fig. 1c). Accordingly, the atom interferometer signal, i.e., the relative population of the two ports, features a bimodal distribution visible in Fig. 2a. However, ambient vibrational noise also results in a displacement of the resonator test mass, which is recorded by the signal retroreflected from the optomechanical resonator (Fig. 1d). The records of the optomechanical resonator make it possible to reconstruct the atomic interference pattern (Fig. 2b). The signal from the optomechanical resonator is constrained to the band of interest. We apply high-pass filters at 0.8 Hz to suppress low-frequency drifts, as well as a digital low-pass filter at 50 Hz, the atom interferometer's corner frequency (see “Methods” section). We subsequently sample it digitally over 60 ms centred around the central light pulse of each interferometer cycle. The phase correction is finally calculated from the signal utilising the acceleration sensitivity function describing the atom interferometer's phase response^{42,43}.

Residual systematic biases can be experimentally analysed as shown for commercial sensors in the ref.³¹.

Using our method, we measure the local gravitational acceleration g in an approximately 22 h-long, interruption-free, measurement series otherwise impossible when operating both sensors alone. By suppressing vibrational noise, our sensor fusion method improves the overall short-term stability by a factor 8 (Fig. 3). Figure 4 illustrates the present and projected features of the atom interferometer, the optomechanical resonator, and the combination of both.

Our optomechanical resonator features a sensitivity comparable to commercial accelerometers, and we expect a large potential for improvements for both quantum-optical devices. The sensor fusion performance is nevertheless limited by low frequency noise (Fig. 4, solid blue trace). It displays a RMS white acceleration noise of $1 \times 10^{-5} \text{ m s}^{-2} \text{ Hz}^{-1/2}$ between 10 and 50 Hz. Pink noise ($\propto f^{-1}$) dominates from 1 to 10 Hz. Below 1 Hz, Brownian noise ($\propto f^{-2}$) processes mainly caused by the optical fibre employed for interrogating the resonator prevail. Since the resonator's sensitivity to accelerations increases quadratically with decreasing mechanical resonance frequency and linearly with optical finesse, there is room for improvements by trading sensitivity against larger bandwidth and dynamic range. We foresee an optimisation of the hybrid sensor (Fig. 4, solid orange trace) by tuning the resonance frequency to 1500 Hz to increase the bandwidth, improving the optical finesse to 1600 by high-reflectivity coating³⁸, and the readout by an order of magnitude as compared to ref.³⁸ by means of spectroscopy techniques developed for ultrastable resonators, e.g., Pound–Drever–Hall locking^{44,45}. Millimetre-sized optomechanical resonators have already demonstrated sensitivities of $1 \times 10^{-6} \text{ m s}^{-2} \text{ Hz}^{-1/2}$ over bandwidths up to 12 kHz.

Additionally, pathways exist for future atom interferometers customised for gravimetry, as discussed in ref.⁴⁶. The sensitivity can be enhanced by operating the device with $T = 35 \text{ ms}$, a cycle rate of 1 Hz, higher-order Bragg processes transferring $4 \cdot k_{\text{eff}}$ and a reduced phase noise of 3 mrad. By improving the atom interferometer and tuning the optomechanical resonator, it is plausible that the intrinsic noise can be lowered to $6 \times 10^{-8} \text{ m s}^{-2} \text{ Hz}^{-1/2}$ under seismic noise as described in the ref.⁴⁷. This target performance is comparable to the noise obtained in a quiet environment with an active vibration isolation¹⁹ and outperforms transportable, commercial devices²³.

Many atomic gravimeters employ rubidium and generate the light for manipulating the atoms by second harmonic generation from fibre lasers in the telecom C-band^{48,49}. The inclusion of the optomechanical resonator therefore requires only minor hardware changes and can be performed with an all-fibred setup. The resonator can be implemented directly into inertial reference mirrors under vacuum, thus improving the mechanical quality factor while supporting miniaturisation of the overall setup. It does not emit notable heat, and is nonmagnetic. Consequently, it does not induce systematic errors due to black body radiation⁵⁰ or due to spurious magnetic fields coupling to the matter waves^{30,51}, and neither do external magnetic fields couple to the resonator test mass. Moreover it can be easily merged with the retroreflection mirror of the atom interferometer. In addition, devices with different resonance frequencies or different orientations will grant access to larger bandwidth and multiple sensitive axes. Last but not least, the small volume of cubic millimetres offers great prospects for being integrated on atom chip sensors⁴⁶, and, hence, a large potential for miniaturisation of the sensor head.

Our method shares analogies with atomic clocks by hybridisation of long-term and short-term references. Beyond this, our optical sensor might be used for compensating inertial

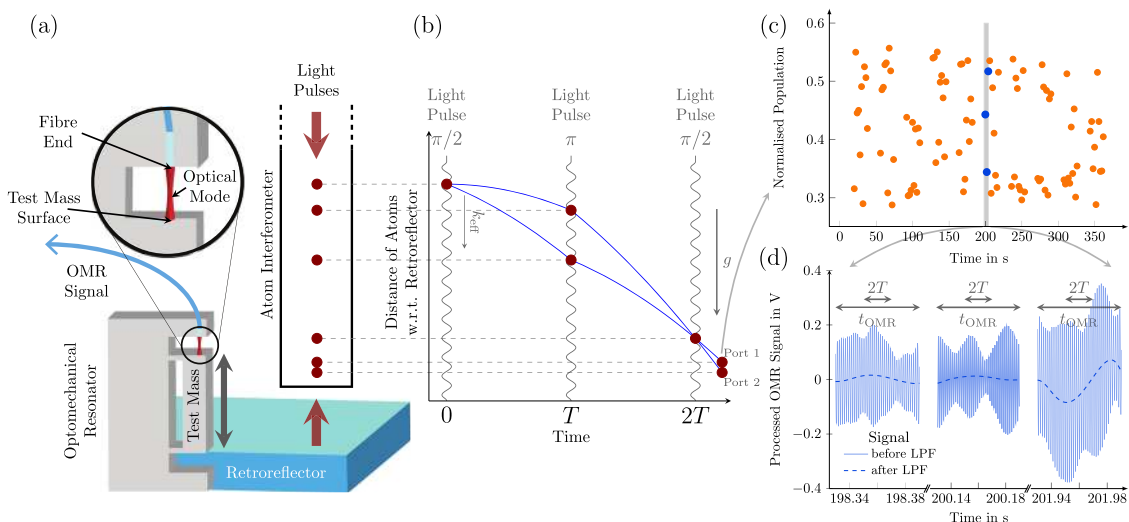


Fig. 1 Representation of measurement principle. **a** Schematic of the experimental setup (not to scale) comprising an optomechanical resonator (OMR) enhancing the optical mode between the flat end of a polarisation-maintaining fibre (light blue), and a side face of the test mass as detailed in the enlarged view and a Mach-Zehnder-type atom interferometer measuring the gravitational acceleration g and **b** its spacetime diagram. The sensor is attached to a retroreflection mirror which rests in strapdown configuration on a platform on the laboratory floor. **c** Ambient vibrations drive the retroreflector’s motion beyond the reciprocal range of the atom interferometer and thus obscure the correspondence between phase and population in the ports 1 and 2. An interferometric fringe can be restored by measuring **d** the test mass motion of the optomechanical resonator and digitally convolving with the atom interferometer’s acceleration response function. Measurement intervals of both devices of durations t_{OMR} and $2T$ are synchronised (details in the “Methods” section). Typical resonator signals are shown before (blue solid line) and after (blue dashed line) low-pass filtering (LPF) which removes the dominant mechanical resonance at 678.5 Hz.

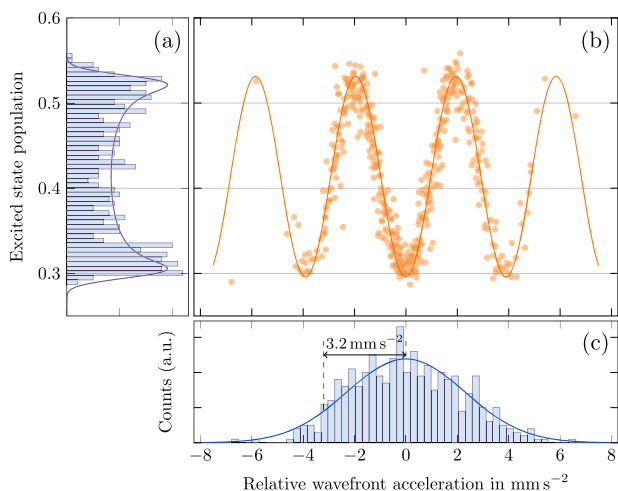


Fig. 2 Exemplary measurement data under vibrational noise. **a** Histogram distribution of the normalised interferometer output ports, **b** a fringe (orange circles) recovered by post-correction based on the resonator signal, and a sinusoidal fit to the corrected data (orange solid line) for a pulse separation time $T = 10$ ms. **c** Ambient vibrations with a Gaussian $1/e$ width of 3.2 mm s^{-2} , if uncorrected, obscure the phase information of the atom interferometer. By convolving the recorded time series of the resonator signal with the interferometer acceleration response function we can recover each data point’s phase information and reconstruct the fringe pattern. Each histogram and the corresponding interferometer response represent a segment of 500 data points.

noise in the resonators of optical clocks, e.g., in transportable setups⁵².

Conclusion. In conclusion, we have demonstrated an atom interferometer enhanced by an optomechanical resonator. We show operation of the atom interferometer under circumstances

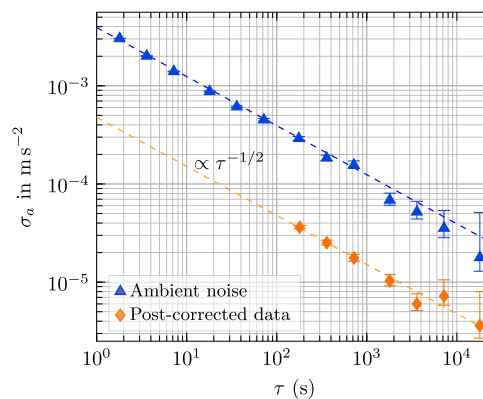


Fig. 3 Analysis of instrument stability. Allan deviations σ_a of estimated ambient noise (blue triangles) and the measured gravitational acceleration from post-corrected data (orange diamonds) as a function of integration time τ . Displayed error bars mark 1σ confidence intervals. Post correction improves the instability at 1 s by a factor of 8 and, here, reduces the measurement time necessary to achieve a target instability by a factor 64. The dashed lines reflect the gain by averaging. We estimate the ambient noise from the phase correction data obtained in our post correction (see “Methods” section).

otherwise impeding phase measurements. Inertial forces on the atoms and on the resonator mirror are measured to the same reference permitting a direct comparison, and high common mode noise suppression in the differential signal. Our method is not restricted to atomic gravimeters and could be beneficial to nearly all atom interferometric sensors and even improve laser interferometers⁵³ in environments with large inertial noise, thus replacing bulky vibration isolation and motion sensors. In particular, the achievable large dynamic range opens up great perspectives for the use of atomic sensors for inertial navigation^{35,54} and airborne gravimetry⁵⁵. Finally, a possible modification of our setup’s topology would ensure that the atom-optics light field is

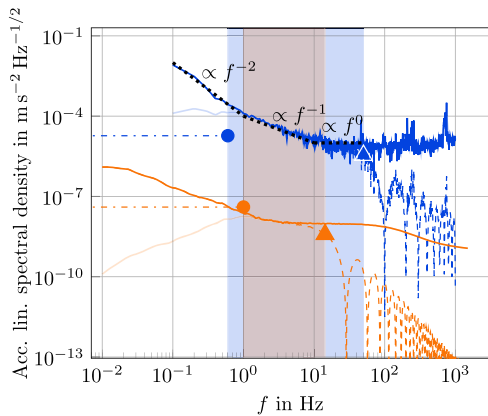


Fig. 4 Sensitivity of sensor fusion setup. Current and anticipated acceleration linear (acc. lin.) spectral density of an atom interferometer enhanced by an optomechanical resonator. Current intrinsic performance (blue dash-dotted line) is achieved using a $T = 10$ ms interferometer with cycle frequency $f_c = 0.6$ Hz, momentum separation of two photon recoils and residual technical noise of 30 mrad. It can be improved with a pulse separation time $T = 35$ ms, a cycle frequency $f_c = 1$ Hz, momentum separation of eight photon recoils and residual phase noise 3 mrad (orange dash-dotted line). Similarly, current optomechanical resonator acceleration sensitivity at quiet conditions (solid blue curve) with a resonance of 678.5 Hz and optical finesse 2 can be optimised by choosing a resonance frequency of 1500 Hz and finesse of 1600 (solid orange curve). Dashed lines indicate the intrinsic noise of the optomechanical resonator weighted by the sensitivity function of the atom interferometer and high-pass filtered at 0.8 Hz (1 Hz) for the current (advanced) scenario to suppress additional noise in the low-frequency band. The shaded areas bounded by f_c (discs) and the atom interferometer’s corner frequency (triangles) mark the respective dominant frequency bands most relevant for optimal postcorrection of seismic noise, and motivate high-pass filtering the resonator signal (light blue and orange solid lines).

reflected directly off a micromechanical test mass. In future experiments, we envisage exciting research on coherent light-mediated coupling of matter waves and mechanical systems^{41,56} with pulsed instead of cw-interaction.

Methods

Atom interferometer. Our setup (Fig. 1a, b), which was employed as a differential gravimeter in the refs. 6,57, comprises a Kasevich–Chu interferometer¹⁷. In a $\pi/2 - \pi - \pi/2$ pulse sequence, stimulated two-photon Raman transitions coherently split, redirect, and recombine matter waves of ⁸⁷Rb. The interferometer phase is determined by measuring the number of atoms in output ports 1 and 2 with state-selective fluorescence detection. To leading order, a constant acceleration \vec{a} of the atoms induces a phase shift

$$\Delta\phi = \vec{k}_{\text{eff}} \cdot \vec{a} \cdot T^2, \tag{1}$$

where $\hbar\vec{k}_{\text{eff}}$ is the photon recoil transferred to the atoms via a Raman process, and T denotes the time between two subsequent light pulses. A chirp of the relative frequency of the lasers cancels the phase induced by acceleration, and is a measure for the latter. The atom interferometer’s response to vibrational noise can be described using the sensitivity formalism⁴². Notably, the response is flat in a band between DC and up to the corner frequency $1/(2T)$, above which it features a low pass behaviour. Typically, the interferometer’s response is adjusted by varying T such that ambient noise induces phase shifts well within one fringe. At quiet conditions, i.e., with an operating vibration isolation system, the interferometer, which we operate at a cycle rate of 0.6 Hz, features a fringe contrast of $\approx 30\%$ and a Raman phase locked loop-limited phase noise of 30 mrad for a time $T = 10$ ms.

Data analysis. In order to suppress systematic shifts independent of the direction of momentum transfer we use the k -reversal method^{58,59}. The interferometer measures ten times in each direction of momentum transfer over a period of 18 s. For each scattering direction, we create histograms out of the normalised output population of the interferometer. Hereby each individual histogram comprises data accumulated over a 9000 s period. From each histogram, we extract the interferometer response’s amplitude and offset⁶⁰ as shown in Fig. 2. We subsequently

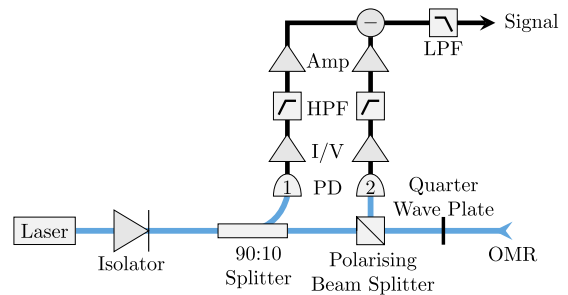


Fig. 5 Displacement readout system for the optomechanical resonator. Laser light split off for intensity noise correction and light reflected back from the optomechanical resonator (OMR) are detected on photo diodes (PD 1 & 2). Both signals are passed to current-to-voltage converters (I/V) followed by high-pass filters (HPF) at 0.8 Hz and are subsequently enhanced by amplifiers (Amp). Finally, the difference signal is digitally low-pass filtered (LPF) at 50 Hz.

extract g for intervals of 180 s (approximately 50 shots per direction) by fitting the postcorrected data to the expected atom interferometer response using the parameters determined by the histogram fit, solely leaving the interferometer phase as a free parameter. After 18,000 s integration we determine a local gravitational acceleration $9.812675 \text{ m s}^{-2}$ with a standard uncertainty of $4 \times 10^{-6} \text{ m s}^{-2}$. We estimate the ambient noise in Fig. 3 from the phase corrections made during postcorrection. Accordingly, the data resembles the underlying ambient acceleration noise after weighting it with the atom interferometer’s transfer function. The first uncorrected value of $\approx 3 \text{ mm s}^{-2}$ per cycle also manifests in the $1/e$ width of the Gaussian-shaped spread in Fig. 2c.

Optomechanical sensor. Mirrors forming the optomechanical resonator, which has a volume on the order of a few hundred mm^3 , are made from the flat tip of a polarisation maintaining fibre and a side face of the fused silica test mass supported by a stiff u-shaped flexible mount, the cantilever (Fig. 1a), following the design of ref. 61. Our sensor features an optical finesse of about two, a resonance frequency of $\omega_0 = 2\pi 678.5$ Hz, and a mechanical quality factor of $Q = 630$. Due to its stiffness the optomechanical resonator can be described as an ideal harmonic oscillator. Below the resonance frequency, displacement of the test mass X as a function of vibration frequency ω linearly depends on the acting acceleration A ,

$$\frac{X(\omega)}{A(\omega)} = -\frac{1}{\omega_0^2 - \omega^2 + i\frac{\omega_0}{Q}\omega}, \tag{2}$$

and is therefore flat. By means of more advanced data analysis, the upper limit of the usable bandwidth can be extended beyond the mechanical resonance. Using adhesive bonding, the resonator is attached to a two-inch square mirror retro-reflecting the light pulses driving the atom interferometer. The resonator’s acceleration-sensitive axis is aligned collinearly with the retroreflector’s normal vector (Fig. 1a) by orienting the outer edges of both devices parallel. The motion of the test mass is read out with a fibre-based optical setup based on telecom components comprising a tunable laser operating at a wavelength near 1560 nm protected by an optical isolator (Fig. 5). The sensor has a quarter wave plate incorporated in its lead fibre thereby enabling us to separate the signal reflected off the resonator using a polarising beam splitter. Additionally, a small fraction of the laser light is split off before the resonator using a 90:10 splitter. Making use of differential data acquisition of photo detectors PD 1 and 2 we can therefore cancel common mode laser intensity noise on the resonator signal. Finally, the processed signal depends on the transmission of the optomechanical resonator and hence the distance between the two reflective surfaces. Consequently, it is a direct measure of the acting acceleration. The optomechanical resonator and the retroreflection mirror are operated under normal atmospheric conditions. We place the mirror with the resonator attached onto a solid aluminium plate in strapdown configuration on the laboratory floor. During the initialisation of the optomechanical sensor, a commercial force-balance accelerometer (Nanometrics Titan) was utilised to perform test measurements for comparison as well as post correction for reference purposes.

Data availability

The data used in this manuscript are available from the corresponding author upon reasonable request.

Received: 1 May 2020; Accepted: 14 October 2020; Published online: 13 November 2020

References

1. Fixler, J. B., Foster, G. T., McGuirk, J. M. & Kasevich, M. A. Atom interferometer measurement of the Newtonian constant of gravity. *Science* **315**, 74 (2007).
2. Rosi, G., Sorrentino, F., Cacciapuoti, L., Prevedelli, M. & Tino, G. M. Precision measurement of the Newtonian gravitational constant using cold atoms. *Nature* **510**, 518 (2014).
3. Spagnolli, G. et al. Crossing over from attractive to repulsive interactions in a tunneling Bosonic Josephson junction. *Phys. Rev. Lett.* **118**, 230403 (2017).
4. Fray, S., Diez, C. A., Hänsch, T. W. & Weitz, M. Atomic interferometer with amplitude gratings of light and its applications to atom based tests of the equivalence principle. *Phys. Rev. Lett.* **93**, 240404 (2004).
5. Bonnin, A., Zahzam, N., Bidel, Y. & Bresson, A. Simultaneous dual-species matter-wave accelerometer. *Phys. Rev. A* **88**, 043615 (2013).
6. Schlippert, D. et al. Quantum test of the universality of free fall. *Phys. Rev. Lett.* **112**, 203002 (2014).
7. Tarallo, M. G. et al. Test of Einstein equivalence principle for 0-spin and half-integer-spin atoms: search for spin-gravity coupling effects. *Phys. Rev. Lett.* **113**, 023005 (2014).
8. Zhou, L. et al. Test of equivalence principle at 10^{-8} level by a dual-species double-diffraction Raman atom interferometer. *Phys. Rev. Lett.* **115**, 013004 (2015).
9. Kovachy, T. et al. Quantum superposition at the half-metre scale. *Nature* **528**, 530 (2015).
10. Pandey, S. et al. Hypersonic Bose-Einstein condensates in accelerator rings. *Nature* **570**, 205–209 (2019).
11. Hamilton, P. et al. Atom interferometry in an optical cavity. *Phys. Rev. Lett.* **114**, 100405 (2015).
12. Jaffe, M. et al. Testing sub-gravitational forces on atoms from a miniature in-vacuum source mass. *Nat. Phys.* **13**, 938 (2017).
13. Bouchendira, R., Cladé, P., Guellati-Khélifa, S., Nez, F. & Biraben, F. New determination of the fine structure constant and test of the quantum electrodynamics. *Phys. Rev. Lett.* **106**, 080801 (2011).
14. Décamps, B., Gillot, J., Vigué, J., Gauguier, A. & Büchner, M. Observation of atom-wave beats using a Kerr modulator for atom waves. *Phys. Rev. Lett.* **116**, 053004 (2016).
15. Parker, R. H., Yu, C., Zhong, W., Estey, B. & Müller, H. Measurement of the fine-structure constant as a test of the standard model. *Science* **360**, 191–195 (2018).
16. Shayeghi, A. et al. Matter-wave interference of a native polypeptide. *Nat. Commun.* **11**, 1447 (2020).
17. Kasevich, M. & Chu, S. Atomic interferometry using stimulated Raman transitions. *Phys. Rev. Lett.* **67**, 181–184 (1991).
18. Peters, A., Chung, K. Y. & Chu, S. Measurement of gravitational acceleration by dropping atoms. *Nature* **400**, 849 (1999).
19. Hu, Z.-K. et al. Demonstration of an ultrahigh-sensitivity atom-interferometry absolute gravimeter. *Phys. Rev. A* **88**, 043610 (2013).
20. Fang, B. et al. Metrology with atom interferometry: inertial sensors from laboratory to field applications. *J. Phys.* **723**, 012049 (2016).
21. Freier, C. et al. Mobile quantum gravity sensor with unprecedented stability. *J. Phys.* **723**, 012050 (2016).
22. Hardman, K. S. et al. Simultaneous precision gravimetry and magnetic gradiometry with a Bose-Einstein condensate: a high precision, quantum sensor. *Phys. Rev. Lett.* **117**, 138501 (2016).
23. Ménotet, V. et al. Gravity measurements below 10⁻⁹ g with a transportable absolute quantum gravimeter. *Sci. Rep.* **8**, 12300 (2018).
24. Bidel, Y. et al. Absolute marine gravimetry with matter-wave interferometry. *Nat. Commun.* **9**, 627 (2018).
25. Stockton, J. K., Takase, K. & Kasevich, M. A. Absolute geodetic rotation measurement using atom interferometry. *Phys. Rev. Lett.* **107**, 133001 (2011).
26. Berg, P. et al. Composite-light-pulse technique for high-precision atom interferometry. *Phys. Rev. Lett.* **114**, 063002 (2015).
27. Dutta, I. et al. Continuous cold-atom inertial sensor with 1nrad/sec rotation stability. *Phys. Rev. Lett.* **116**, 183003 (2016).
28. Hinton, A. et al. A portable magneto-optical trap with prospects for atom interferometry in civil engineering. *Philos. Trans. R. Soc. A* **375**, 20160238 (2017).
29. Chen, Z., Lim, H. M., Huang, C., Dumke, R. & Lan, S.-Y. Quantum-Enhanced Velocimetry with doppler-broadened atomic vapor. *Phys. Rev. Lett.* **124**, 093202 (2020).
30. Gouët, J. L. et al. Limits to the sensitivity of a low noise compact atomic gravimeter. *Appl. Phys. B* **92**, 133–144 (2008).
31. Merlet, S. et al. Operating an atom interferometer beyond its linear range. *Metrologia* **46**, 87 (2009).
32. Lautier, J. et al. Hybridizing matter-wave and classical accelerometers. *Appl. Phys. Lett.* **105**, 144102 (2014).
33. Geiger, R. et al. Detecting inertial effects with airborne matter-wave interferometry. *Nat. Commun.* **2**, 474 (2011).
34. Barrett, B. et al. Dual matter-wave inertial sensors in weightlessness. *Nat. Commun.* **7**, 13786 (2016).
35. Cheiney, P. et al. Navigation-compatible hybrid quantum accelerometer using a Kalman filter. *Phys. Rev. Appl.* **10**, 034030 (2018).
36. Peters, A., Chung, K. Y. & Chu, S. High-precision gravity measurements using atom interferometry. *Metrologia* **38**, 25–61 (2001).
37. Merlet, S. et al. Comparison between two mobile absolute gravimeters: optical versus atomic interferometers. *Metrologia* **47**, L9–L11 (2010).
38. Cervantes, F. G., Kumanchik, L., Pratt, J. & Taylor, J. M. High sensitivity optomechanical reference accelerometer over 10 kHz. *Appl. Phys. Lett.* **104**, 221111 (2014).
39. Pisco, M. et al. Opto-mechanical lab-on-fibre seismic sensors detected the Norcia earthquake. *Sci. Rep.* **8**, 6680 (2018).
40. Hunger, D. et al. Resonant coupling of a Bose-Einstein condensate to a micromechanical oscillator. *Phys. Rev. Lett.* **104**, 143002 (2010).
41. Camerer, S. et al. Realization of an optomechanical interface between ultracold atoms and a membrane. *Phys. Rev. Lett.* **107**, 223001 (2011).
42. Cheinet, P. et al. Measurement of the sensitivity function in a time-domain atomic interferometer. *IEEE Trans. Instrum. Meas.* **57**, 1141–1148 (2008).
43. Bonnin, A., Zahzam, N., Bidel, Y. & Bresson, A. Characterization of a simultaneous dual-species atom interferometer for a quantum test of the weak equivalence principle. *Phys. Rev. A* **92**, 023626 (2015).
44. Pound, R. V. Electronic frequency stabilization of microwave oscillators. *Rev. Sci. Instr.* **17**, 490–505 (1946).
45. Drever, R. W. P. et al. Laser phase and frequency stabilization using an optical resonator. *Appl. Phys. B* **31**, 97–105 (1983).
46. Abend, S. et al. Atom-chip fountain gravimeter. *Phys. Rev. Lett.* **117**, 203003 (2016).
47. Peterson, J. Observations and Modeling of Seismic Background Noise, USGS Open-File Report 93-322, <https://doi.org/10.3133/ofr93322> (U. S. Geological Survey, Albuquerque, New Mexico, 1993).
48. Luo, Q. et al. A compact laser system for a portable atom interferometry gravimeter. *Rev. Sci. Instrum.* **90**, 043104 (2019).
49. Theron, F. et al. Frequency-doubled telecom fiber laser for a cold atom interferometer using optical lattices. *Opt. Commun.* **393**, 152–155 (2017).
50. Haslinger, P. et al. Attractive force on atoms due to blackbody radiation. *Nat. Phys.* **14**, 257–260 (2017).
51. Hu, Q.-Q. et al. Observation of vector and tensor light shifts in ⁸⁷Rb using near-resonant, stimulated Raman spectroscopy. *Phys. Rev. A* **97**, 013424 (2018).
52. Grotti, J. et al. Geodesy and metrology with a transportable optical clock. *Nat. Phys.* **14**, 437–441 (2018).
53. Niebauer, T. M., Sasagawa, G. S., Faller, J. E., Hilt, R. & Klotting, F. A new generation of absolute gravimeters. *Metrologia* **32**, 159–180 (1995).
54. Jekeli, C. Navigation error analysis of atom interferometer inertial sensor. *Navigation* **52**, 1–14 (2005).
55. Bidel, Y. et al. Absolute airborne gravimetry with a cold atom sensor. *J. Geod.* **94**, 20 (2020).
56. Karg, T. M., Gouraud, B., Treutlein, P. & Hammerer, K. Remote Hamiltonian interactions mediated by light. *Phys. Rev. A* **99**, 063829 (2019).
57. Albers, H. et al. Quantum test of the Universality of Free Fall using rubidium and potassium. *Eur. Phys. J. D* **74**, 145 (2020).
58. McGuirk, J. M., Foster, G. T., Fixler, J. B., Snadden, M. J. & Kasevich, M. A. Sensitive absolute-gravity gradiometry using atom interferometry. *Phys. Rev. A* **65**, 033608 (2002).
59. Louchet-Chauvet, A. et al. The influence of transverse motion within an atomic gravimeter. *N. J. Phys.* **13**, 065025 (2011).
60. Varoquaux, G. et al. How to estimate the differential acceleration in a two-species atom interferometer to test the equivalence principle. *N. J. Phys.* **11**, 113010 (2009).
61. Gerberding, O., Cervantes, F. G., Melcher, J., Pratt, J. R. & Taylor, J. M. Optomechanical reference accelerometer. *Metrologia* **52**, 654 (2015).

Acknowledgements

We thank H. Ahlers, J. Lautier-Gaud, L. Timmen, J. Müller, S. Herrmann, S. Schön, K. Hammerer, D. Rätzl, P. Haslinger, and M. Aspelmeyer for comments and fruitful discussions and acknowledge financial support from Deutsche Forschungsgemeinschaft (DFG) within CRC 1128 (geo-Q), projects A02, A06, and F01 and CRC 1227 (DQ-mat), project B07, and under Germany's Excellence Strategy—EXC-2123 QuantumFrontiers—390837967 (research unit B02). D.S. acknowledges support by the Federal Ministry of Education and Research (BMBF) through the funding program Photonics Research Germany under contract number 13N14875. This project is furthermore supported by the German Space Agency (DLR) with funds provided by the Federal Ministry for Economic Affairs and Energy (BMWi) due to an enactment of the German Bundestag under Grant No. DLR 50WM1641 (PRIMUS-III), 50WM1137 (QUANTUS-IV-Fallturm), and

50RK1957 (QGYRO), and by “Niedersächsisches Vorab” through the “Quantum-metrology and Nano-Metrology (QUANOMET)” initiative within the project QT3, and by “Wege in die Forschung (II)” of Leibniz University Hannover.

Author contributions

W.E., E.M.R., C.S., and D.S. designed the atom interferometer and its laser system. L.L.R., H.A., D.N., and D.S. contributed to the design of the atom interferometer and its laser system and realised the overall setup. A.R., M.M., L.K., L.C., R.S., C.B., and F.G. designed, built, and tested the optomechanical resonator and designed the readout laser system. A.R., C.M., D.T., and É.W. built and characterised the laser system for readout. L.L.R., F.G., L.K., and A.R. implemented the optomechanical resonator in the atom interferometer setup. L.L.R., H.A., D.N., and A.R. operated the final experimental setup. Sv.A., M.G., and C.S. contributed to the data acquisition system utilised for post correction. A.R., D.N., C.S., and L.L.R. performed the analysis of the data presented in this manuscript. L.L.R., D.S., and F.G. drafted the initial manuscript. A.R., C.M., C.S., D.T., É.W., E.M.R., and L.K. provided major input to the manuscript and all authors critically reviewed and approved of the final version.

Funding

Open Access funding enabled and organized by Projekt DEAL.

Competing interests

Related to the patent *Optomechanical Inertial Reference for Atom Interferometers* (WO 2020/168314 A1) filed by the University of Arizona (UA), L.L.R. (UA affiliate), F.G. (UA affiliate and inventor), E.M.R. (inventor), and D.S. (inventor) declare competing financial

interests. The patent covers the use of opto-mechanical systems as inertial references for atom interferometry. All other authors declare no competing interests.

Additional information

Correspondence and requests for materials should be addressed to D.S. or F.G.

Reprints and permission information is available at <http://www.nature.com/reprints>

Publisher's note Springer Nature remains neutral with regard to jurisdictional claims in published maps and institutional affiliations.



Open Access This article is licensed under a Creative Commons Attribution 4.0 International License, which permits use, sharing, adaptation, distribution and reproduction in any medium or format, as long as you give appropriate credit to the original author(s) and the source, provide a link to the Creative Commons license, and indicate if changes were made. The images or other third party material in this article are included in the article's Creative Commons license, unless indicated otherwise in a credit line to the material. If material is not included in the article's Creative Commons license and your intended use is not permitted by statutory regulation or exceeds the permitted use, you will need to obtain permission directly from the copyright holder. To view a copy of this license, visit <http://creativecommons.org/licenses/by/4.0/>.

© The Author(s) 2020